AOARD-09-4058 / FA2386-09-1-4058

Mechanisms for Visual Detection of Small Targets in Insects

Final Performance Report
December 1, 2009

David O'Carroll
Discipline of Physiology
School of Medical Sciences
University of Adelaide
Adelaide SA 5005
AUSTRALIA
+61 8 8303 4435

In collaboration with:

Patrick Shoemaker
Tanner Research, Inc.
825 South Myrtle Ave.
Monrovia CA 91016
USA
(626) 471-9786

Report Documentation Page

Form Approved
OMB No. 0704-0188

1. REPORT DATE	2. REPORT TYPE	3. DATES COVERED
02 DEC 2010	**FInal**	**26-03-2009 to 26-06-2010**

4. TITLE AND SUBTITLE
Mechanisms for Visual Detection of Small Targets in Insects

5a. CONTRACT NUMBER
FA23860914058

5b. GRANT NUMBER

5c. PROGRAM ELEMENT NUMBER

6. AUTHOR(S)
David O'Carroll

5d. PROJECT NUMBER

5e. TASK NUMBER

5f. WORK UNIT NUMBER

7. PERFORMING ORGANIZATION NAME(S) AND ADDRESS(ES)
University of Adelaide,Department of Physiology,S. A. 5005,Australia,AU,5005

8. PERFORMING ORGANIZATION REPORT NUMBER
N/A

9. SPONSORING/MONITORING AGENCY NAME(S) AND ADDRESS(ES)
AOARD, UNIT 45002, APO, AP, 96337-5002

10. SPONSOR/MONITOR'S ACRONYM(S)
AOARD

11. SPONSOR/MONITOR'S REPORT NUMBER(S)
AOARD-094058

12. DISTRIBUTION/AVAILABILITY STATEMENT
Approved for public release; distribution unlimited

13. SUPPLEMENTARY NOTES

14. ABSTRACT
The grantee investigated insect visual detection of small targets against a cluttered, moving background. The work focused on deducing neural mechanisms that underlie this ability, to an understanding of the computational principles. Electrophysiology examined the complex function of small-target sensitive neurons. Experiments explored the receptive field properties and underlying mechanisms involved in target detection, suggested the form of computational models, and focused anatomical investigations. Conceptual models were translated into numerical models that can be evaluated in simulations under a variety of conditions and compared with biological systems.

15. SUBJECT TERMS
Insect Flight Control, Insect Vision

16. SECURITY CLASSIFICATION OF:			17. LIMITATION OF ABSTRACT	18. NUMBER OF PAGES	19a. NAME OF RESPONSIBLE PERSON
a. REPORT	b. ABSTRACT	c. THIS PAGE			
unclassified	**unclassified**	**unclassified**	**Same as Report (SAR)**	**26**	

Note on period of performance:

The base period for this grant had an intended period of performance of 1 MAR 2009 to 30 NOV 2009; however, because this initial increment of funding supported work through JAN 2010, the results reported herein encompass the period 1 MAR 09 – 31 JAN 2010.

1 Objectives

The primary objective is to further improve understanding of the computational principles that underlie the response characteristics of wide-field STMDs. A secondary objective is to achieve a more in-depth empirical characterization of cell response, particularly with regard to details that bear on the limits of performance as small moving target detectors, and on unresolved questions regarding computational mechanisms. Specific goals are defined with respect to:

1. *Rectifying Transient Cells*: The goals are to determine whether or not neurons of this class in fact lie on the neural pathway leading to STMDs; to obtain a more detailed characterization of physiology and anatomy, and to perform modeling and analysis that accounts for details of the physiology and the putative role of RTCs in STMD processing not yet addressed.
2. *Nonlinear Facilitation for Long-Range Spatiotemporal Correlation in STMDs*: The goal is to determine experimentally if STMDs exploit the longer-range spatiotemporal correlations that arise due to the constraint that target motion occurs along continuous paths, and to elucidate the nature of the computations by which this is achieved.
3. *Further Characterization of STMD Behavior*: The goals include determination of the mechanism of the immense amplification required to support vigorous responses to sub-pixel targets; how inhibitory responses within the receptive field, or on earlier pathways to the STMDs, suppress responses to other features; and the range of 'non-target' stimuli (e.g. features of the background image) that produce responses from the STMD.
4. *Improved 'Standard' Front End for Modeling*: The goal is to determine to what degree, and how, photoreceptor properties increase target detectability, to enable improved modeling of target detection.
5. *Improved Model for Wide-Field STMDs*: The goal is to develop a more capable wide-field STMD model that incorporates the spatiotemporal filtering characteristics of early vision, followed by rectification and adaptation inherent in the RTC, and a final stage based on a temporal nonlinear facilitation mechanism. One benchmark for this model will be to explain target motion detection without relative motion cues.

There have been no changes to these objectives during this reporting period.

2 Status of Effort

In the O'Carroll laboratory at the University of Adelaide, electrophysiological experiments have focused heavily on the issue of facilitation in wide-field STMDs, which has been a major topic addressed in the dissertation of PhD student Douglas Bolzon. A fundamental hypothesis regarding wide-field STMDs, formulated some years preceding,

is that they exploit the spatiotemporal correlations due to small target motion along continuous paths in order to obtain higher-confidence detection of targets; testing this hypothesis is the basis of Objective 2 above. Bolzon ran a set of experiments in which target paths of different lengths were presented in the receptive field of the neuron CSTMD1, in order to examine the build-up of facilitation. Further experiments examined the roll-off of response to targets whose motion ended within the receptive field, in order to distinguish between facilitation and the alternate hypothesis of long latencies and/or time constants contributing to the time course of changes in activity. This work is detailed in Section 3.3.2.

Further experiments were also designed and performed to confirm the local nature of facilitation, using stimuli with discontinuous target paths. This work was initiated during the 3-14 December 2009 visit of Patrick Shoemaker to the O'Carroll laboratory. The visit was focused on the development of a specific experimental protocol to test the locality hypothesis, and the implementation of this protocol in the stimulus-generation and display hardware. Subsequently, pilot experiments run with this protocol by PhD student James Dunbier were analyzed and discussed, also during the visit. This work is discussed in Section 3.3.3.

Experimental work was also conducted to verify aspects of the elementary STMD (ESTMD) models of Wiederman et al, in which moving scenes with embedded targets and including possible natural distractors were displayed to dragonflies while recordings were made from the CSTMD1 neuron. Details are given in Section 3.4 below.

In the modeling domain, optical modeling of neural contrast (Section 3.3.1) was conducted at the University of Adelaide. Conceptual development of a model incorporating prior work on ESTMDs, but also accounting for the several levels of spatial inhibition observed in wide-field STMDs, was also carried out and is described in Section 3.5. This work has illuminated questions about the nature of this inhibition, which will drive upcoming experiments on STMDs.

Finally, Shoemaker has re-initiated and advanced prior work on the computational primitives afforded by the electrical properties of NMDA synaptic receptors. This is a continuation of research previously performed under AFOSR contract FA9550-04-1-0283. The current round of work has been pursued under the joint support of the present grant and Air Force SBIR contract FA8651-07-C-0099, because the NMDA receptor nonlinearity has been construed as a plausible biophysical mechanism for: 1) Nonlinear facilitation that may play a significant role in the amplification and small-target selectivity observed in STMDs; and 2) The fundamental nonlinear interaction at the heart of directional motion detection in wide-field visual motion processing (relating to the objectives of the SBIR contract).

This work has focused primarily on the analysis of stationary equations to elucidate the conditions associated with NMDA receptor-mediated bistability and amplification, both in single-compartment and dendrite models. It has incorporated prior results in two areas, of which the PI was unaware during previous work on NMDA receptors: 1) The role of inward-rectifying potassium (Kir) channels in establishing the resting membrane potential as well as their association with $GABA_B$ receptors in neurons; 2) prior mathematical work on bistability in dendrites, which, although aimed at the effects of slow calcium currents, is also largely applicable to NMDA-induced bistability. This phase of the effort is largely complete and has been written up in a manuscript; novel

results are described in Section 3.2. Work on bistability and amplification under dynamic conditions will take place in the early months of the first option period of the grant.

The analysis of NMDA receptor-mediated behavior has informed modeling efforts to account for facilitation seen in wide-field STMDs, in satisfaction of the second goal listed under project objectives. NMDA-based models will be developed in subsequent periods.

3 Accomplishments / New Findings

3.1 Rectifying Transient Cells

No new findings in this area.

3.2 Nonlinear Facilitation for Long-Range Spatiotemporal Correlation in STMDs

3.2.1 Bistability and amplification mediated by NMDA receptors

The effort under this task, carried out by Shoemaker, includes general theoretical work on bistability and amplification in neurons and neural structures associated with NMDA synaptic receptors. In the whole neuron, the electrical effects of NMDA receptors necessarily depend on the characteristics of other membrane conductances, as well as cytoplasmic resistivity when cellular structures like dendrites are considered. These effects are reflected in the dynamical characteristics of the instantaneous operating regime of a neuron or neural structure – i.e., mono- vs. bistability – and the particular characteristics of the system within a given regime, including amplifying properties when monostable.

A significant update of the prior work on this topic has been the inclusion of the effects of a class of channels known as the *inward-rectifying potassium* or Kir channels. These have been implicated as contributing significantly to the resting potassium conductance [9] (which dominates the resting membrane conductance in most neurons), and recent work has also shown that Kir channels are activated by an important class of inhibitory synaptic receptors, the $GABA_B$ receptors [3]. Kir channels show a pronounced nonlinearity that cannot be explained by the Goldman diffusion/drift model [4]; their conductance falls off rapidly with increasing membrane potential for outward currents (i.e., at membrane potentials above the potassium reversal potential).

The effects of Kir conductance has been examined by developing an *ad hoc* model for its electrical characteristics, as illustrated in Figure 1 below, and simulating neurons and neural structures that include Kir as well as NMDA and resting ionic conductances in the membrane.

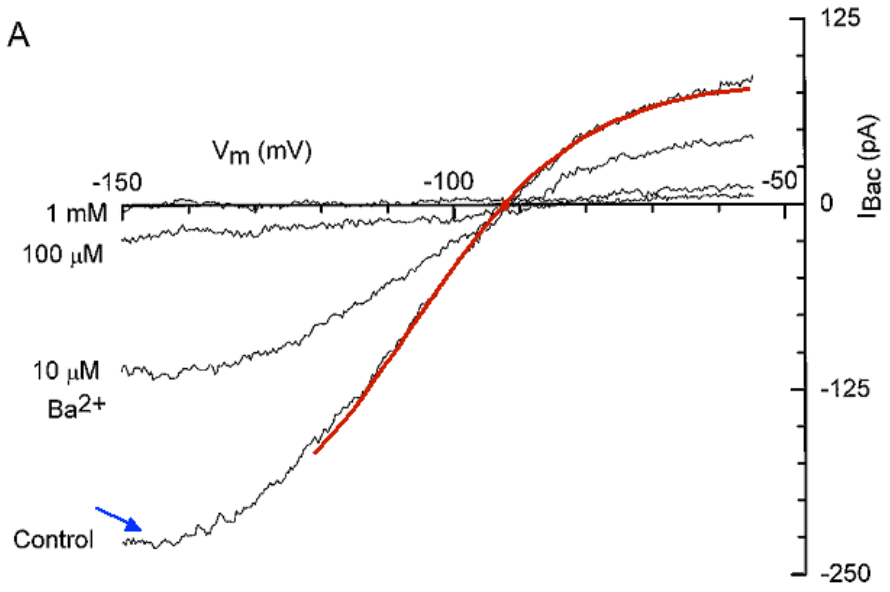

Figure 1: Fit of an *ad hoc* model for the current-voltage relation of Kir channels to data obtained in voltage-clamp experiments by Sodickson and Bean [15]. Abcissa is membrane potential and ordinate is current; the experiment examined blocking of the channels with barium but included an unblocked control, to which the function was fit. The red line depicts this fit. The function takes the form
$I_{Kir}(V_m ; V_{r0,} G_{Kir}) = G_{Kir} \cdot d \cdot [\tanh\{ (V_m - V_{r0} - c)/d \} - e]/[1 - \tanh^2\{c/d\}]$,
where *tanh* denotes hyperbolic tangent, the reversal potential V_{r0} and the conductance (slope) at the reversal potential G_{Kir} are free parameters, and the remaining parameters *c*, *d*, and *e* are fixed at the values –13.73mV, 25mV, and 0.5, respectively. The fit to empirical data was achieved with G_{Kir} = 4.4nA/V and reversal potential V_{r0} = -92mV.

Numerical experiments with single-compartment models show that the presence of open Kir channels increases the area in parameter space over which the system is bistable. Figure 2 below shows the bistable regions in a compartment with NMDA conductance (modeled with the Jahr-Stevens equation [8]) and a second type of membrane conductance. Results for three classes of non-NMDA conductance are shown: one is the superlinear Goldman model, the second a linear conductance, and a third is the (sublinear) Kir model. The parameter space in the graph is spanned by the reversal potential of the non-NMDA channels, and the ratio of NMDA to non-NMDA conductance (measured at the reversal potential for each channel).

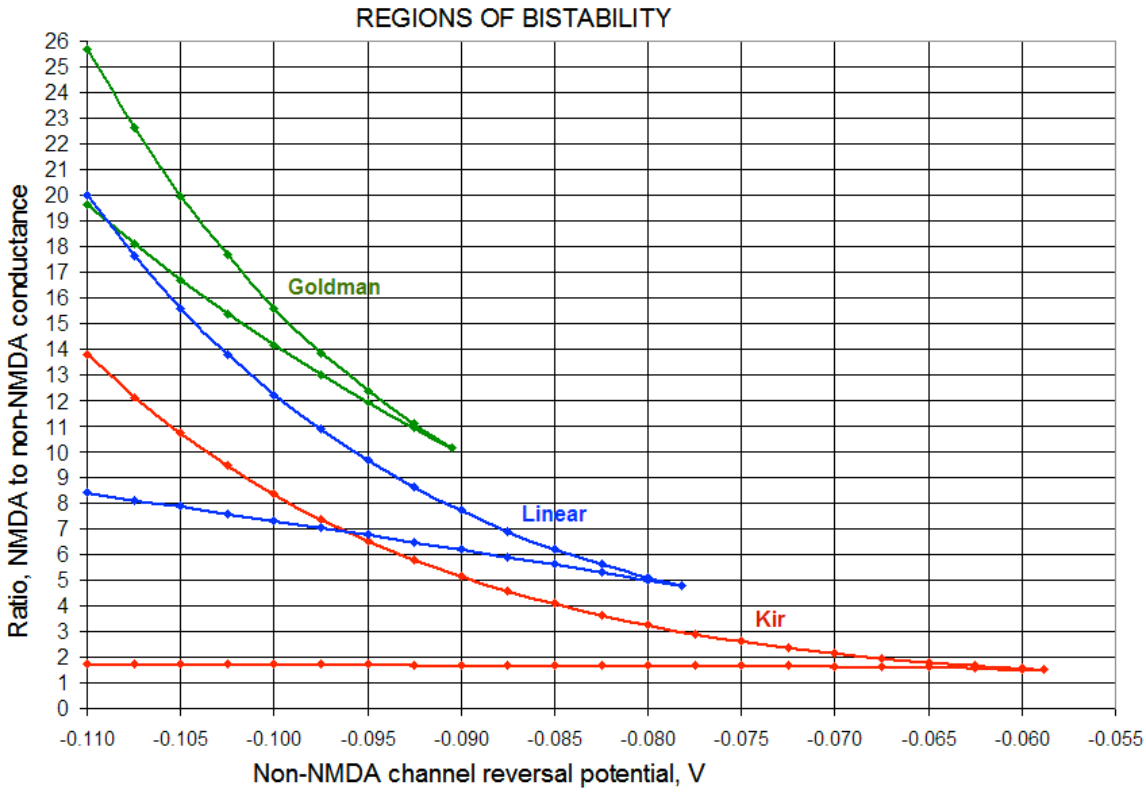

Figure 2: Regions in which a bistable regime prevails in a single electrical compartment with NMDA receptor and a second class of ionic membrane conductance. Results are shown for three models for the non-NMDA conductance: green is for the Goldman model, blue for a linearized model, and red for the Kir model. The abscissa is the reversal potential of the non-NMDA channels, and the ordinate the ratio of NMDA to non-NMDA conductance (measured at the reversal potential for each channel type).

The fact that Kir channels are associated with $GABA_B$ synapses suggests that in neurons that have receptors of both types, there is a powerful ability to directly regulate the transient dynamical state of the cell via synaptic inputs. Additionally, coactivation of both classes of synapses allows a degree of control over amplification associated with the NMDA receptor nonlinearity, and thus with nonlinear facilitation that may have the NMDA receptor as its biophysical substrate. A useful high-gain regime is found to extend from the vicinity of the cusp bifurcation (pointed termination of the bistable region) depicted in Figure 2. Characterization of this amplification is proceeding at present.

Another update of previous work has been the identification and extension of prior work on the bistability of individual dendrites by Gutman and coworkers [1][6][7]. They considered a dendritic model based on a one-dimensional cable equation, in which bistability arises from a nonmonotonic membrane current-voltage relation with three zeros of the current, due to slow, persistent inward calcium currents. The theory, however, can be applied equally well to NMDA receptor channels acting in concert with other membrane conductances.

Gutman considered the boundary-value problem in which a dendrite is sealed (i.e., allows no current flow) at the distal end, and voltage-clamped at the proximal end,

defining boundary conditions on the governing cable equation. Several important theoretical results that were obtained for this model [6] can be summarized as follows:

1. Below a critical dendritic length, the solution of the stationary cable equation (membrane potential V_m as a function of axial position χ) is unique for all values of the proximal clamp voltage, and the relationship between the current flowing into the dendrite and the clamp voltage is single-valued;
2. For dendrites longer than this critical length, the solution is *not* unique for some range of values of the clamp voltage. The current flowing into the dendrite may assume any of two or more values for any clamp voltage within this range. Furthermore, this voltage range increases as the length of the dendrite increases, and it becomes semi-infinite for a semi-infinite dendrite;
3. The *number* of possible solutions within this voltage range also increases as dendritic length increases, but all except two of these solutions are unstable. The stable solutions each feature a monotonic dependence of V_m on χ. There are thus two possible *stable* values of current into the dendrite for any clamp voltage within the range, and it is proper to speak of *intrinsic bistability of a dendrite as a whole*.

To give an idea of the character of these solutions, Figure 3 depicts simulation results for current flowing into a dendrite as a function of the proximal clamp voltage, for a cable-like dendrite with a particular density of active NMDA and $GABA_B$ receptors per unit length. Total dendritic length Λ in non-dimensionalized coordinates is a parameter.

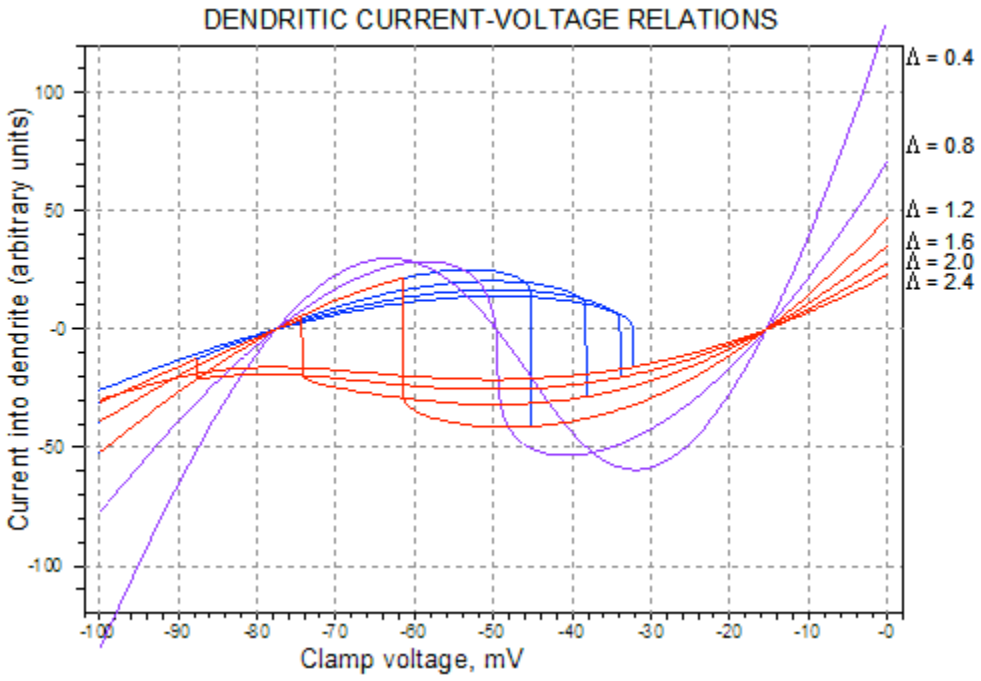

Figure 3: Relations between the current flowing into a dendrite with active NMDA and $GABA_B$ receptors and the potential (relative to extracellular space) of a proximal voltage-clamp load, with dendritic length Λ in non-dimensionalized coordinates as a parameter. Monostable relations are shown in purple, and bistable in red and blue, with red representing the lower stable branch and blue the upper, in the bistable region.

In the present project, these results have been extended in several areas:

1. A conceptual error in a prior analysis of the minimum critical dendritic length supporting bistability [1] has been identified and a more useful approximation of this length has been developed;
2. The bistability of dendrites under a mixed or Robin-type boundary condition, associated with a finite somatic load at the proximal end, has been examined. This boundary condition is a more realistic approximation to dendritic physiology than the voltage-clamped or Dirichlet boundary condition applied by Gutman [6]. When the electrical load becomes finite, the critical length for dendritic bistability is found to decrease;
3. The existence of bistable regimes induced by series cytoplasmic resistance in dendrites whose membrane current-voltage relation does not have multiple zeros has been demonstrated. (In the case of such *load-induced bistability*, there is however some region in the distal dendrite in which the relationship between an injected current and the local membrane potential *does* have three zeros.)

Finally, work is proceeding on the analysis of amplification in dendrites with NMDA receptors. Further details will appear in reports for subsequent periods of the grant.

3.2.2 Application to facilitation in wide-field STMDs

The application of these findings to the problem of facilitation in wide-field STMDs is in the planning stage. Such an STMD is assumed to receive input from retinotopically-distributed, elementary target-sensitive units such as those modeled by Wiederman et al. [17]. The first step will be to model local facilitation as due to amplifying nonlinearity (as opposed to bistable behavior) associated with NMDA receptors. This will follow the general concept introduced by Mel et al. [11][12][14], in which activation of a set of NMDA receptors that are in electrical proximity (i.e., are localized together within a portion of the dendritic tree) induces a high-gain regime in the local membrane and results in substantially greater depolarization at the base of the dendritic tree than would occur if the active receptors were distributed uniformly throughout the tree. This concept will be combined with the assumption of a retinotopic mapping from the elementary STMDs onto the dendrites of the wide-field cell, such that retinotopic distance correlates with electrical distance between receptors. In this way, the motion of a target along a continuous path will sequentially excite neighboring inputs, and induce facilitation in the wide-field target cell.

The tree structure of dendrites, however, has implications for this retinotopic mapping that need to be considered in the formulation of a model. In particular, when a finite subset of the presynaptic units converge on a primary branch and its distal ramifications, it will necessarily contain units whose neighbors in retinotopic space do not synapse onto the same branch. There is therefore a need for overlap in the ‘receptive fields’ of dendritic ramifications to ensure there are no discontinuities in response throughout the receptive field.

The central test of the hypotheses behind such a model will be whether the free parameters of the retinotopic mapping, including overlap and synaptic strengths/synaptic densities, can be chosen – given the predetermined kinetics of the NMDA receptor – to account for the observed spatiotemporal characteristics of facilitation,

To be examined in the subsequent grant periods will be ‘propagating wave’ models for facilitation, in which the facilitatory ‘wave speed’ matches the velocity optimum in the space of the retinotopic mapping onto the target cell. Such a wave, in principle, might be either electrical or chemical. A cursory review of the propagation of ‘passive’ potentials (i.e., induced by approximately linear membrane characteristics) suggests the speed of propagation is too fast; however, with the presence of significant nonlinearity with the NMDA receptor, active propagation of depolarization (as in the propagation of action potentials by voltage-gated channels) needs to be considered in greater depth.

3.3 Characterization of facilitation in dragonfly STMD neurons

3.3.1 Optical modeling of neural contrast

Our earlier data for STMD neurons, particularly the robust responses to targets much smaller than the effective size of an individual photoreceptor receptive field (i.e. ‘sub-pixel’ targets) are indicative of massive amplification in the underlying motion pathway. How much amplification is required and how is this achieved? To address this question quantitatively we need to know the magnitude of photoreceptor responses to the targets in question. While we have yet to conduct experiments to directly measure the scale of the photoreceptor response at the limits of STMD performance, we have now modeled the optics of the eye to take into account the photoreceptor size and shape, and the optical blur introduced by diffraction at the ommatidial lens. This model shows that at the limits of STMD performance, targets generate a ‘maximal neural contrast’ of less than 1%. We define neural contrast as the difference in photon catch between a photoreceptor centered exactly on a target of 100% contrast with its background, and that of a photoreceptor at a large enough distance from the target that it views only the background. Note that because optical blur distributes some of the energy associated with the target onto nearest neighbor photoreceptors, the actual effective contrast for near neighbor ‘pixels’ in the neural processing pathway will always be less than the neural contrast by this definition (hence our designation as ‘maximal’ neural contrast). If we now take account of the measured V/Log(I) functions for light adapted photoreceptors (i.e. the response, V, as a function of stimulus intensity, I), this model predicts photoreceptor responses of less than 1mV (depending on the local luminance of the near surround pattern). Our ongoing experiments with photoreceptor recordings and stimulation with identical targets to those used in STMD recordings aim to quantify this directly. However, our preliminary recordings reveal standard deviation of the membrane potential in an unstimulated photoreceptor to be of at least similar magnitude to this maximal target response, so that the transition of a target across the receptive field of a single receptor would be expected to produce a bump in membrane voltage so small that it would be buried in the noise.

3.3.2 Facilitation within the receptive field of STMD neurons

The above observation leads to the hypothesis that in addition to local processing to achieve selectivity for small features, STMDs require an additional non-linear mechanism such as feed-forward facilitation in the direction of travel of a target, in order to allow integration of what is effectively a single pixel signal across numerous pixels in the time domain.

To test the hypothesis, PhD student Douglas Bolzon conducted an experiment on the CSTMD1 neuron in dragonfly, which we are able to record from reliably for periods of up to an hour or more. The experiment design tests whether the receptive field revealed

by drifting a small target is influenced by a facilitation mechanism. i.e. if local responses are stronger if the target moves towards that location for a prior period, compared with those where the target commences motion at the same location. We first characterized the receptive field of the CSTMD1 neuron by drifting a near-optimal sized target (0.9 degree square subtense) upward across the entire stimulus screen (approx. 70 degrees vertical extent) at 21 different azimuthal trajectories (Figure 4). We then identified the azimuthal location of the receptive field hotspot (at around 10-15 degrees west of the animal's frontal midline) and drifted a target upwards along this line (as illustrated in Figure 4) multiple times, in each case starting from below the bottom of the screen, so that the trajectory length was maximized.

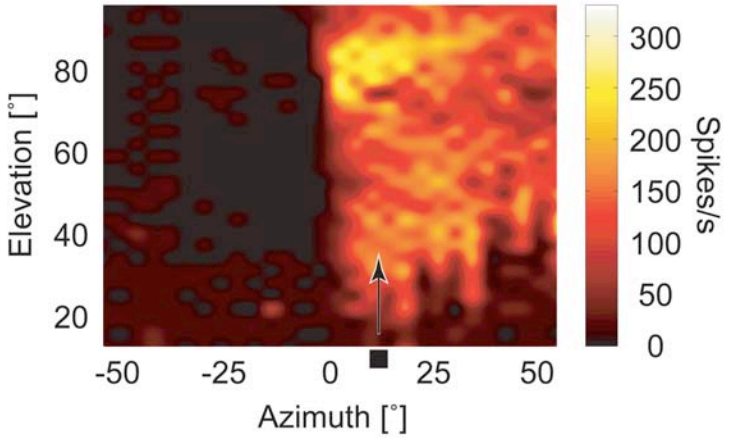

Figure 4: Receptive field response of CTSMD1, illustrating the trajectory of the small target used to reveal facilitation in the response. A single 0.9° square target drifted upwards at 55°/s from the bottom to the top of the visual display (control). The receptive field map in this case is built up from 21 successive upward sweeps of the target, commencing each time at a different azimuth. The target illustrated shows the approximate location used for subsequent facilitation experiments, aligned with the region of maximum sensitivity (yellow colours), i.e. the receptive field 'hotspot'.

The results of this control experiment are illustrated in Figure 5A. After identification of the azimuthal location of the receptive field hotspot, subsequent stimuli were drifted along this trajectory, but commencing at different elevations (again expressed relative to the animal's frontal midline). The control experiment (Figure 5A) commenced at 10 degrees elevation. Subsequent tests (Figure 5B-E) commenced at 37, 52, 56 and 60 degrees elevation, the latter being just below the receptive field hotspot.

The data for these tests (black histograms) is shown in Figure 5 (B-E) over-plotted against the control data from Figure 5A (in gray). In each case, it is clear that the response accumulates gradually over time (and corresponding to approximately 25 degrees in angular position) before matching the same level as the control data, which then varies according to location of the stimulus. By Figure 5E, the response barely matches the control level by the time the target leaves the upper edge of the receptive field (at around 85 degrees elevation). Given that the target speed was 55 degrees/second, this indicates that a 'steady state' response level is only achieved after motion for ~500ms and covering >25 degrees in angular extent.

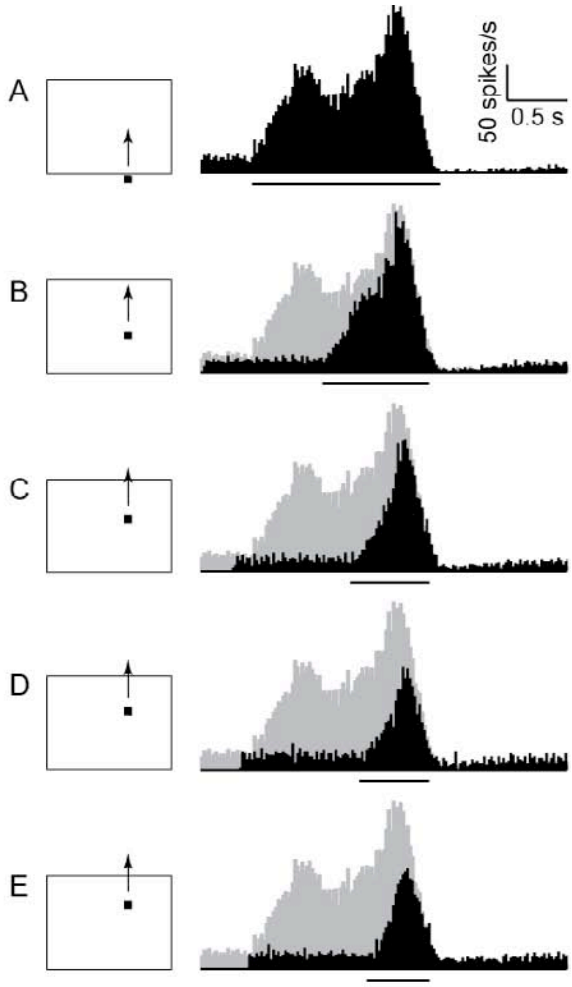

Figure 5: (A) Receptive field response to the control trajectory (i.e. full path length, see Figure 4). Data are shown as spike histograms averaged across at least 20 trials, in 20 ms bins. (B-E) A target appeared within the receptive field and drifted vertically (see pictograms). Responses for target start locations (black histograms) were aligned with the corresponding location of the control response (grey histogram) for comparison. Each successive histogram shows the target starting at more vertical locations on the display.

To quantify this further we need to account for the variation in response rate as a function of stimulus position, i.e. the underlying structure of the receptive field. We can use the spike rate in each bin in the control experiment above (Figure 5A) as a normalizing value to reveal the time course of response facilitation regardless of local receptive shape (i.e. underlying local gain). Figure 6 shows the data from Figure 5B-E after dividing each bin by the value for the equivalent spatial location of the target in Figure 5A. As can be seen responses confirm the qualitative observations above, rolling on very slowly, with a time course of several hundred milliseconds. It is evident from the similarity in the basic shape of each curve, despite the differences in local response rate due to the underlying receptive field, that this slow-response roll on follows a similar time course independently of spike rate. Interestingly, if the slow roll-on were due to a simple time-dependence (e.g. due to a low-pass filter with a very long time constant) we

would expect responses to roll-on exponentially to the steady state level. While the later part of each curve shows some exponential build up towards a plateau level, individual traces from each neuron that we have studied and at each location shows responses that initially build linearly or even supra-linearly with time. The specific shape of this time course is, however, quite variable from trial to trial and from neuron to neuron (Figure 6 is averaged from 20 trials in a single neuron).

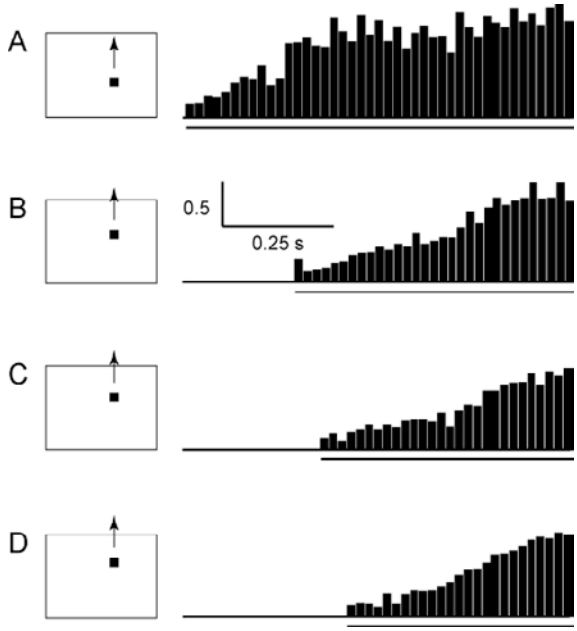

Figure 6: (A) Spike histograms obtained from Figure 5 (20 ms bins) but now showing responses for a target starting within the receptive field (see pictograms) divided by the response for a target that drifted through the whole receptive field after position alignment, resulting in a relative response (see Figure 5B, black histogram divided by grey histogram). i.e. a zero bin value indicates no response compared to the control at the same location, while 1.0 represents an equal response. (B-D) Each successive histogram shows the relative response to a target starting at more vertical locations on the display and thus receptive field. Black bars beneath the histograms represent the duration of the target motion in each case, aligned by the absolute time in the upper trace so that each bin represents the same location on the screen.

To quantify the time course further, we repeated the analysis in Figure 6 for a total of 7 neurons, for both the upward trajectories as used in Figure 5 and Figure 6, and for horizontal trajectories that pass from left to right across the receptive field hotspot at 70 degrees elevation. The latter provides an interesting basis for comparison, because the receptive field boundary is sharply defined at the midline (azimuth=0 degrees; see Figure 4). To the left of this, the neuron display little or no response to moving targets.

We then averaged the normalized response rate across these recordings and from several different start locations in each case. The technique is problematic because of the low spontaneous firing rate of the neurons and variability in neuronal response, which lead to a risk of zero or near zero values in the control experiment, particularly near the receptive field boundaries. Because the normalization by receptive field weight is divisive, this leads to large error values when we attempt to average across neurons.

Larger bin-sizes reduce this risk, but diminish our resolution of the time course of response build-up. In the end we discarded data from the 3 most variable neurons before computing the average time course for the remaining 4, illustrated in Figure 7, with a compromise bin-size of 20 ms.

As noted above, the early part of the response time course for upward motion (0-100 ms after onset) is distinctly supra-linear, and error (SEM) values are small despite the small data set. This is less evident for the horizontal (left to right) scans, which rise approximately linearly for the first 200 ms. Over a longer term, however, both directions of motion produce responses that plateau after 400-500ms. Exponential fits to the data reveal an overall time to 50% response level; (T_{50}) of around 200ms (see insets in Figure 7) and thus a time constant of at least 200-300 ms.

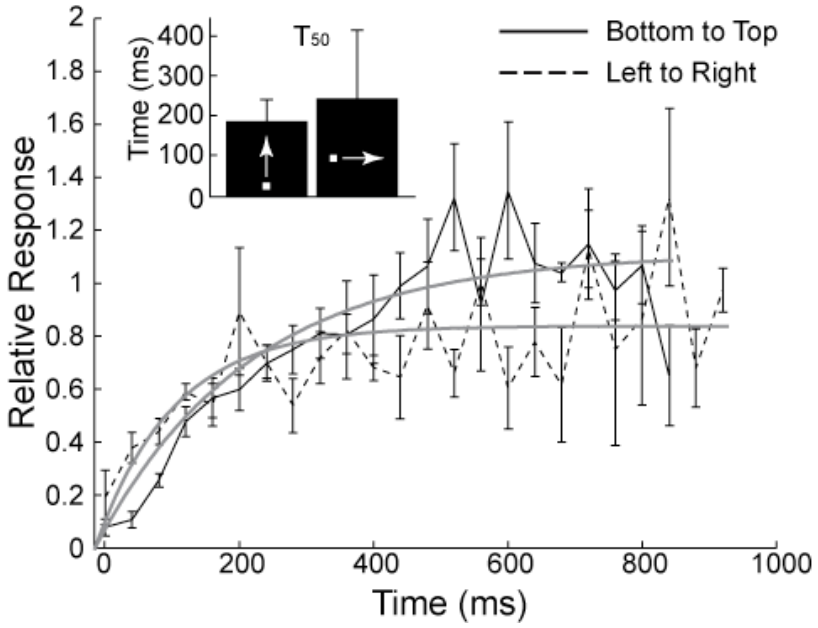

Figure 7: Time course in roll-on of normalized average response of CSTMD1 for a small 0.9° square target drifted at 55°/s from left to right (dashed line; N=4, n=) and bottom to top (solid line). An exponential function was fitted to the data by nonlinear optimization for each direction. T_{50} was calculated for each direction. Data is presented as mean (N=4) ± s.e.m.

The horizontal motion experiment above is particularly noteworthy because we see a slow facilitation relative to the control experiment even when the target starts just to the left of the mid-line. Since the only difference in this case, compared with control, is the distance which the target passes across a region of the receptive field that itself induces no excitation of CSTMD1 itself, we conclude that the roll on is unlikely to result from a global facilitation mechanism operating within this higher order neuron, and is more likely due to interactions between input elements operating at an earlier stage in the target motion pathway.

Nevertheless, the above experiments provide only tantalizing evidence (based on the shape of the response roll on in the first 200ms) that the response that we see is not simply the result of sluggish kinetics in the input pathway – for example a long delay in the underlying local motion detection operation or simply a low-pass filter mechanism

operating after local motion computation. To test this alternate hypothesis, we drifted targets along the same trajectories as in Figure 5A, but this time stopped the target motion either within the receptive field hot-spot (Figure 8A) or just beyond the hot-spot (Figure 8B). Under both conditions, response decays rapidly toward or below baseline activity levels. After allowing for the local receptive field, we see that this decay is much shorter than the rate of response onset, by a factor of 5 (time constants ~40-50 ms). This asymmetry argues strongly against the response being simply low-pass filtered (although even a 40-50 ms decay rate is relatively slow for insect visual neurons).

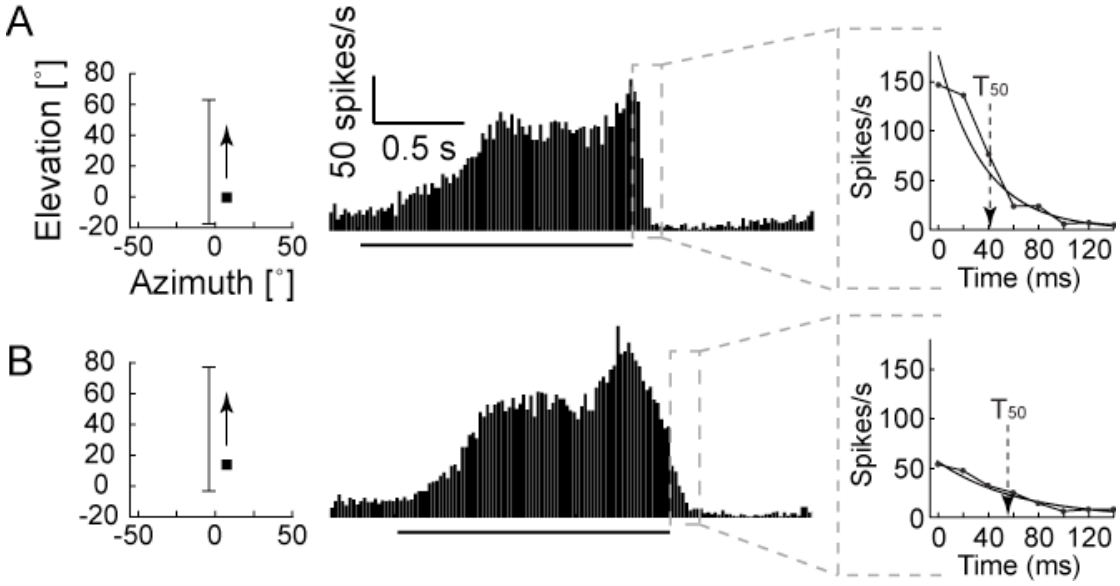

Figure 8: (A) Spike histogram (20 ms bins) showing the response for a single 0.9° square target drifted at 55°/s vertically through the receptive field (N=4). We see gradual response facilitation and rapid response decay when the target disappears. The black bar beneath the histogram indicates the duration the target was within the receptive field, also shown in the pictogram (elevation [°]). (B) Response for a target that started and stopped more dorsally within the receptive field. We fitted an exponential function to the response decays and calculated T50.

3.3.3 Discontinuous path analysis: Is facilitation local or global?

From the above sequence of experiments (forming the last chapter of Douglas Bolzon's PhD thesis, currently under completion, and an associated paper in preparation) we conclude that CSTMD1 is likely to utilize a second-order facilitation mechanism operating after local motion detection. However it is not clear from the data in Figure 4-Figure 8 whether this is a local mechanism, operating between local motion detecting elements, or a global mechanism that depends only on the activity of the CTSMD neuron itself. While a second-order motion detection mechanism spreading away from a site of activation and acting locally to boost responses of nearby motion detecting elements is an attractive hypothesis, in principle, such facilitation could be a property of the higher order neuron itself – e.g. an increase in global gain that depends on activation history.

The observation that horizontal trajectories (Figure 7) evoke slow roll-on compared with controls even when the target commences just outside the receptive field argues

against the latter, but to develop additional evidence, we also designed an experiment that explicitly tests the locality of facilitation seen in wide-field STMDs. In this experiment, the total motion energy (i.e., total path length traversed by a small target moving at a given rate) is maintained constant, but the paths in a series trials are divided into discontinuous segments of successively smaller lengths (Figure 9). The supposition is that, if the buildup of facilitation were a global phenomenon in a wide-field STMD, then division of a target traversal into discontinuous segments should make little difference in the level of response after the neuron has reached full activation. Conversely, if facilitation is localized, presumably due to electrical or chemical isolation in the dendritic tree, then facilitation would have to build anew when the target jumps from one region to a significantly distant region of the receptive field.

This stimulus class was designed as follows, and was targeted in particular toward the CSTMD1 neuron found in dragonfly, although the user interface has sufficient flexibility that it may be applied to any wide-field STMD that is responsive to vertical target motion. As noted, CSTMD1 is strongly responsive to targets moving in a front-to-back direction or an upward direction; its excitatory receptive field is enlongated vertically and located adjacent to the midline in retinotopic space. To avoid binocular interactions and take advantage of the receptive field shape, the stimulus was designed to employ vertical target motion. On the stimulus display, five vertical pathways are evenly spaced in azimuth within an area that is defined by the user, following spatial characterization of the receptive field using existing stimulus suites. Small targets, with user-definable size and speed, move along these pathways. As a control, the target may be made to traverse the five pathways one at a time over the entire length of each, while the neural response is recorded. There is a user-defined rest period between each traversal, and each traversal after the first occurs over a path that is at least two pathways distant in azimuth from the prior traversal.

These pathways may also be broken into *n* discontinuous segments, where *n* is any integer not divisible by the number of pathways (five). After traversing one segment, the target jumps instantaneously to another pathway, again at least two pathways distant in azimuth from the prior segment, and traces another segment beginning at the same elevation as the end of the prior segment. After *n* segments have been traversed, the target reaches the top of the stimulus area, and the user-defined rest period ensues. Following the rest period, target motion begins again at the bottom of the stimulus area on a new segment at least two pathways distant from the previous. This procedure continues until the full length of each of the five pathways has been traversed. The total distance and the azimuthal locations traversed are thus the same in the control experiment or for any trial using any number of segments *n*, as illustrated below in Figure 9. Because the receptive fields of wide-field STMDs are generally non-uniform, the locations and sequence of the segments are recorded so that responses from trial to trial may be compared relative to position in the receptive field.

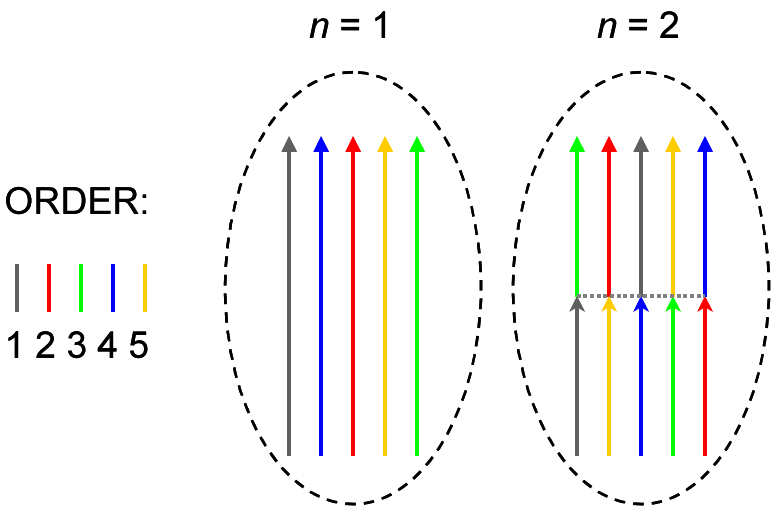

Figure 9: Schematic diagram representing an experiment to determine how local the phenomenon of facilitation is for a small target moving within the receptive field (dashed ovals) of a wide-field STMD. Five vertical pathways are defined on the display so as to fall within the cell's receptive field. Traversal of these pathways by small targets are indicated by colored arrows, with the order of the traversals from bottom to top coded by color as indicated at left. The diagrams at center and right illustrate two experimental trials performed on the same receptive field. The parameter *n* indicates the number of (discontinuous) segments traversed per pathway; *n* = 1 signifies the control experiment in which the full vertical distance is traversed in a single segment, while *n* = 2 illustrates an case in which the traversals occur in two discontinuous segments.

The stimulus macro implementing this protocol was written, debugged, and put into use during Shoemaker's site visit to Adelaide in December 2009. Shoemaker, O'Carroll & Wiederman then trained a commencing PhD student, James Dunbier, in CSTMD1 recording from the dragonfly and application of this protocol. James has subsequently obtained preliminary data using this technique in 4 successful neuron recordings. Data analysis is ongoing and incomplete at the time of writing this report, due in part to the need to prepared work for presentation at the annual meeting of the Australian Neuroscience society at the end of January. Nevertheless preliminary data analysis strongly supports the hypothesis for non-linear facilitation between local motion detectors in the presynaptic pathways.

Preliminary data are illustrated in Figure 10. In this case, the target trajectory was limited to end at the hotspot in the receptive field (see Figure 4) so that responses from bottom to top of the trajectory tended to always be increasing over time due to the receptive field. This is evident from the sharp build up in the response at the end of the first of the 5 stimulus segments (gray marker) seen in Figure 10A. Despite this globally maximal response at the end of this time point, however, the response falls to zero as soon as the target is relocated to next segment (red marker). Note that the 4th trajectory in this sequence (blue marker) is the closest to the first, but even though the neuron is again firing strongly by the end of the 3rd trajectory (green marker), again we see a 'silent' period in the neuronal response, persisting for several hundred milliseconds into this

segment. Close examination of the underlying membrane potential indicates that between spikes, resting potential may be as much as 10mV below the resting level towards the end of the sequence, suggestive of the accumulation of a strong inhibitory drive over time (possibly an activity-dependent mechanism).

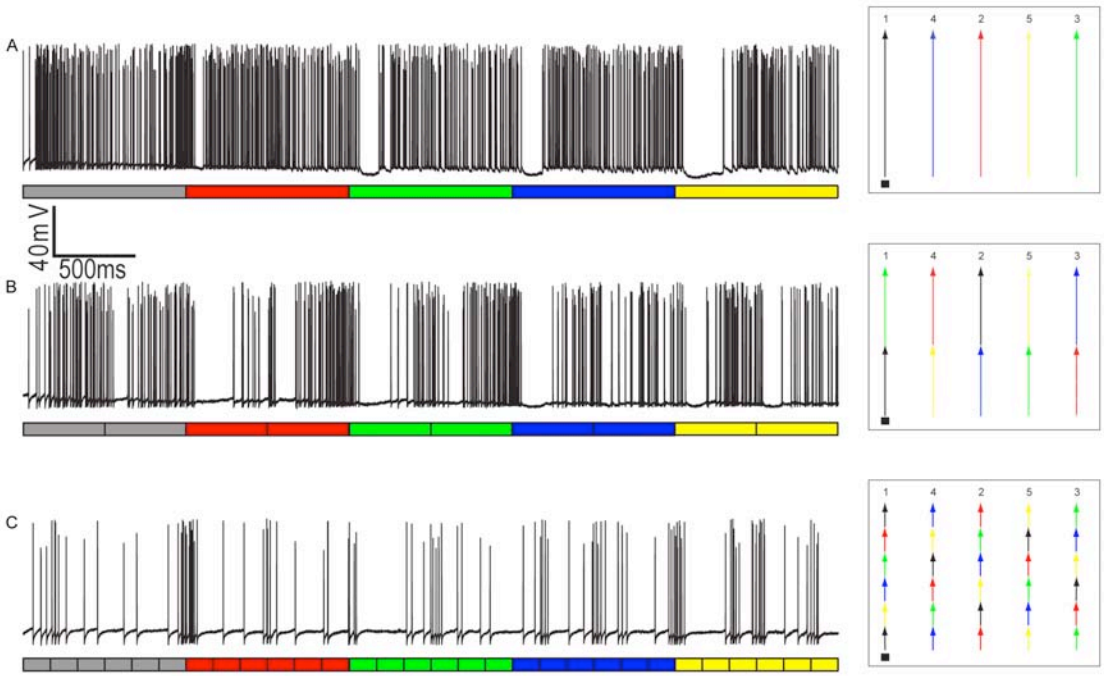

Figure 10: (A) shows the raw response of CSTMD1 to the control experiment, where the target moves along 5 nearby paths, always in a vertical direction, finishing approximately level with the receptive field 'hot spot' on path 1 (gray time marker). Note the emergence of an apparent inhibitory drive over time, evident from the 'silent' periods when the target commences a new trajectory and the gradual decline in the resting membrane potential over time. (B) As indicated by the colored time points, this trace shows the same target sweeping the same 5 paths, but this time with each path segmented into halves, and with the target jumping a minimum of 2 adjacent paths between each segment (e.g. from the left most to the center path on the first sweep) as per Figure 9. As can be seen, overall responses are weaker in this condition. (C) Dividing paths into smaller segments (6 per path, lower trace) reduces responses even further.

Figure 11 shows the results of analyzing multiple different repetitions of the multiple path experiment (Figure 9) and then taking the averaged spike rate for each location in the sequence and plotting them at the appropriate position, relative to the receptive field (hot spot evident at top left). As can be seen, the discontinuous paths always take a similar time after each 'jump' to regain control experiment levels and so overall local responsiveness is strongly reduced when the path length becomes short. This shows conclusively that responses are not facilitated by global activity level of the neuron. Indeed, the 'silent' periods between segments shows the opposite – that the only obvious global influence based on recent activation of CSTMD1 is the slow build up of inhibitory drive evident from hyperpolarization in the raw data (Figure 10).

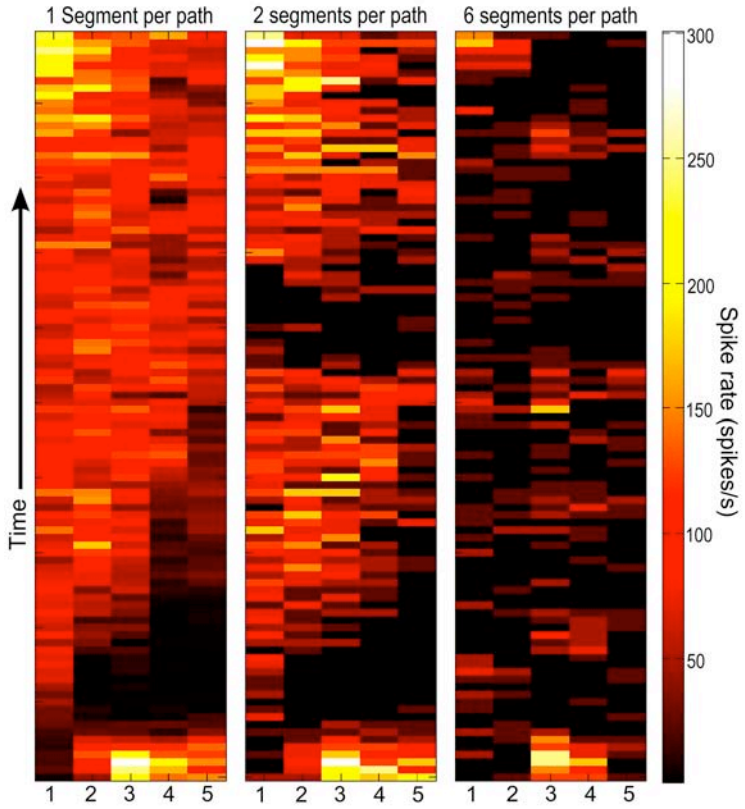

Figure 11: Receptive fields reconstructed from full length (left) and discontinuous path experiments (middle, right). Left panel shows the control experiment, where the target moves along each of the 5 paths for a full 1000ms period (actual path order was 1,3,5,2,4) across a subset of the receptive field of CSTMD1 (see Figure 4). In the middle panel path segment length was halved (500ms per segment) and in the right panel there were 6 segments per location (167 ms/segment). As can be seen, overall response is much weaker as path length declines, even though the stimulus spend the same total time sweeping the same set of locations in all 3 cases.

3.4 Experimental verification of RTC-based model predictions of CSTMD1 response to natural scenes based on an improved standard front-end model

In two further modeling developments, we have elaborated models that we produced for earlier work to study responses to targets embedded in visual clutter in an attempt to account for the higher-order interactions within the receptive field of the dragonfly CSTMD1 neuron. CSTMD1, like the STMDs described in our earlier work, responds to optimal targets (i.e. ideal size) embedded in natural scenes, even if such features move at the same speed as the background pattern. As the RTC-based model produced by Steve Wiederman for his PhD work (and published in Wiederman et al. [17]) is able to explain this based on potent local inhibition mechanisms, we wanted to elaborate the model to allow us to test predictions for which features in natural scenes might be expected to recruit ‘false’ positive responses from this type of mechanism from a higher-order (wide-field) STMD neuron like CSTMD1. We have now developed an elaboration of that

model, with an improved ‘front-end’ based on the photoreceptor model that we published recently [10].

To test the predictions of this model against a neuron like CSTMD1 is not trivial however, because the latter has a relatively complex receptive field (as seen in Figure 4). Hence while a model may be used to predict which local features may recruit responses (including artificial targets inserted into the images), it is difficult to associate a given response of the neuron with those features. Furthermore, a complete model for this higher order receptive field structure is in itself not a trivial undertaking (see Section 3.5), as it needs to account for binocular inhibitory interactions and other long-range inhibition mechanisms (shown in the earlier PhD work of Bolzon, as published with partial support from this present project; see Section 5.1) In partial mitigation of this problem, we selected subsets from natural scenes - strips with limited vertical extent - from 3 scenes (one of which is illustrated in Figure 12) which contained a few features distributed along the horizontal length of the pattern that were predicted by the Wiederman et al. model [17] to generate weak responses.

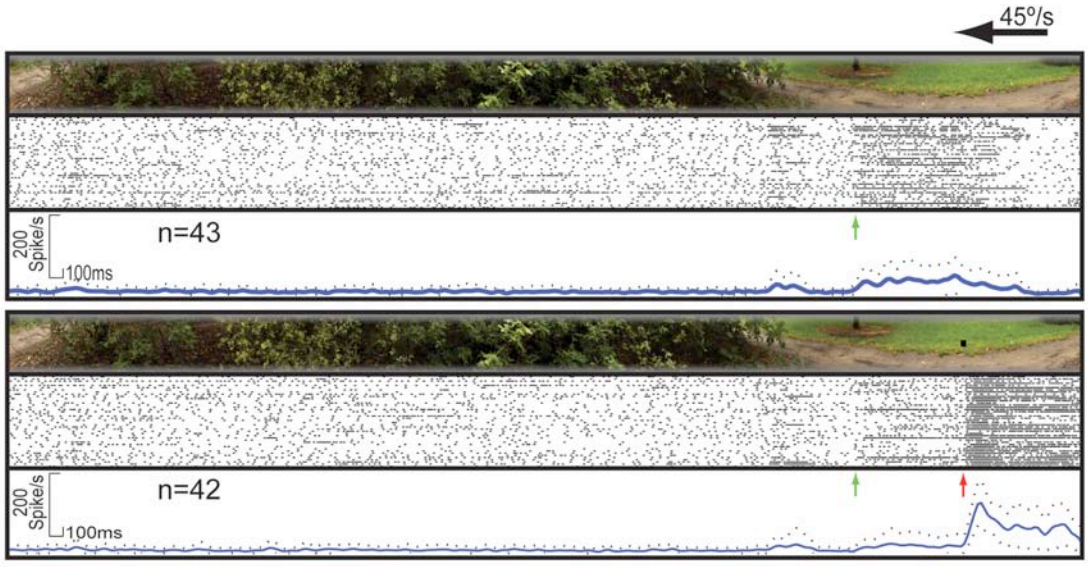

Figure 12: CSTMD electrophysiological responses to a real-world scene. In this case, two versions of the scene were presented, with (above) and without (below) an artificial target inserted into a region where it generates large local contrast.

We then tested CSTMD1 by presenting these images moving at 45 degrees per second across the receptive field. Each image was tested in two versions, with and without an artificial black target embedded into the scene at a location where it provides a strong contrast with nearby background features. This feature matches the preferred size of the neuron and thus provides a control that allows us to reveal the response to an optimal feature. In Figure 12, the data from the neuron are plotted in two ways: as raster plots, where each dot represents the time of an action potential (spike) generated in a sequence of repeated presentations of the same scene; and as binned data in histogram form (blue lines), averaged across all times. Both plots have been scaled so that the data align with the *time* at which the corresponding vertical column of the image was centered on the hot spot of the neuron receptive field. Thus, because of the limited vertical extent

of the scenes, strong responses in the neuron are most likely to be associated with features at the corresponding horizontal location of the scene.

As can be seen from the data for both images, in the control experiment, the neuron produces the most vigorous spiking responses at the same time that the artificially embedded feature passes the receptive field centre (indicated by red arrow, lower trace). However, several features of the underlying scenes also produce weaker responses when presented without the embedded targets. In the first image above (Figure 12), for example, a small tree towards the upper right hand side of the image is truncated by our reduction of this scene to a narrow strip. While in the original full-height image this tree is large enough that it is not predicted to provide a response from the STMD model, in this truncated version its visible base is short enough that it does predict weak responses, and this is observed (green arrow in the upper trace). To the left of this tree, a small outlying group of leaves on the right hand side of the bush also contain a local feature predicted by the model to produce possible response, and again there are weak responses evident in many individual traces as this feature passes the receptive field. When the artificial target is included in the image, however, the response to these same features (particularly the tree base) is reduced, presumably because the target is present in the binocular field of the eye, thus producing response inhibition at the same time as these weak features pass the receptive field 'hotspot'.

These preliminary experiments allow us to make two key conclusions:

- Firstly, spike responses of CSTMD1 to the majority of features in several different scenes tested are very weak compared with responses to an optimal feature artificially embedded in the scene. This confirms experimentally, for the first time, conclusions reached using our earlier modeling approach that the elementary small target motion detectors (ESTMDs) based on rectifying transient cells can be tuned to respond to targets whilst remaining largely insensitive to the structure of most elements in natural scenes.
- Secondly, the presence of longer-range inhibitory mechanisms evident from our recently published data for CSTMD1 [2] need to be incorporated into a model for a large field STMDs before we can fully explain the complex interactions between different features within scenes.

3.5 Improved Model for Wide-Field STMDs

In an attempt to address the second point above, we constructed a more elaborated STMD model in Matlab, based on known or proposed neural elements along the target-detection pathway. The model is outlined in Figure 13. Briefly, it consists of our improved standard front-end (stage i) that mimics the dynamic range compression and adaptive properties of local visual processing in fly photoreceptors. For a complete description, see Mah et al. [10] and Wiederman et al. [16]. This is then followed (stage ii) by local target selectivity that exploits the ESTMD model that we described in our earlier work, based on a rectifying transient cell (RTC) [17]. The model then incorporates a longer-range higher order inhibitory mechanism (stage iii), with a larger scale, as proposed by our recent analysis of CSTMD1 responses to paired target stimuli [2]. One aim of the present model effort was to determine the scale and magnitude for this component that best matches the observed physiological data, by simulating these 'two target' experiments. An additional model component (stage iv) is required to fully

account for the inter-ocular (binocular) inhibitory interactions described in 3.4 above. As at the time of writing this report, work on this stage is incomplete, but will continue if the option periods of this project are funded. Finally, local interactions between each of these stages are summed across a receptive field weighted locally (stage v) to mimic the measured CSTMD1 receptive field (or that of other STMD neurons that the same model might be applied to in future work).

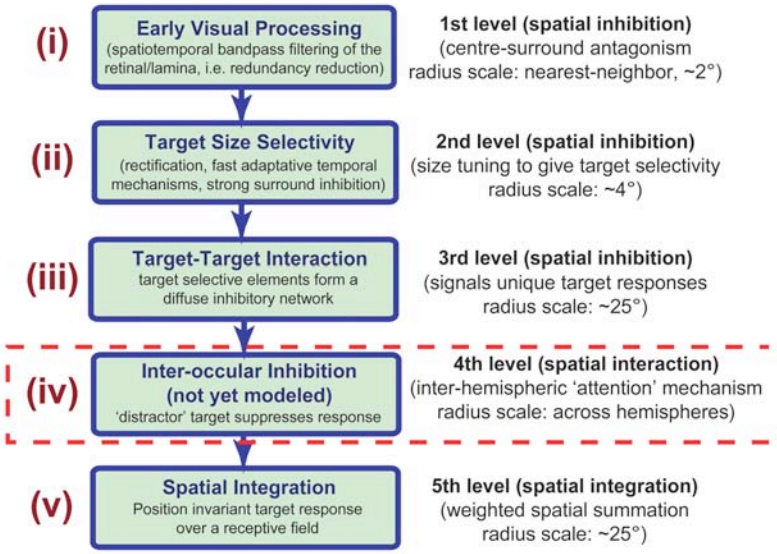

Figure 13: Conceptual organization of a higher order CSTMD1 model The model includes levels of spatial interactions, in order to explain observed response characteristics. The CSTMD1 model builds on previous bio-inspired efforts including high dynamic range inputs, green spectral sensitivity and hexagonal sampling. The model extensions include target-target interactions and spatial integration (levels iii & v). It is simulated in MATLAB with each level representing known or proposed neural elements along the target-detection pathway

In our modeling efforts with this approach so far, we have tuned the stage (iii) interactions by simulating the 2-target experiments carried out (with partial support from the present project) by PhD student Bolzon (and now published in Bolzon et al. [2]). For convenience, we summarize these results in Figure 14. There are two key observations here: firstly that a very potent inhibition operates between local ESTMDs, on a scale of 2-3 ommatidial separation. Second, that there is a longer-range inhibitory mechanism also in operation, extending an influence well outside this local mechanism. (>15 degrees) From the results in Figure 14, an interesting question arises. Is the inhibitory interaction from the second target due to the target's *luminance* being present in a diffuse inhibitory surround (centre-surround antagonism)? Or is the inhibition dependent on the presence of the *form of a target* within this surround? To examine whether this second option is a plausible, we added target-target interactions to our modeling efforts and compared this with the observed electrophysiological data.

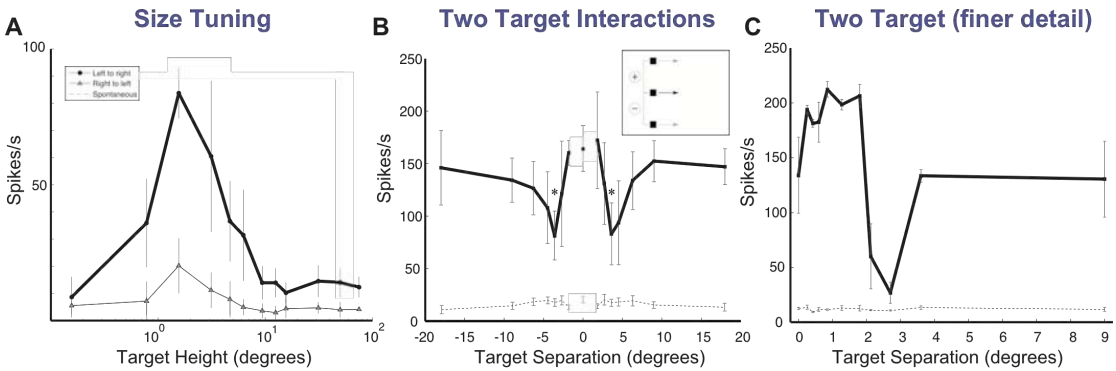

Figure 14: Electrophysiological data reproduced from our recently published papers. (A): Guerten et al. [5]. CSTMD1 is size selective for targets of around 2°. (B&C) Bolzon et al. [2]. Two targets are simultaneously drifted across the stimulus monitor at varying vertical separation. In B, even at large distances the spiking response is reduced compared to the control (single target, i.e. 0° separation) indicating long-range inhibition. In C (higher resolution target separation) CSTMD1 response increases, as the two targets seeming become a single, more optimal size, before inhibitory influences are then revealed as separation increases beyond 2°.

Target size selectivity (level ii) in this model is, in part, derived from surround inhibition of strong luminance dependent signals (rectified on and off channels). Following this, we have modeled a diffuse target-target inhibitory network (level iii). We varied both the spatial extent and the strength of this diffuse inhibitory network. Inter-occular inhibitory mechanisms, as observed in the electrophysiological responses, have not yet been included in this work (level iv). Finally, changing the types of spatial integration (level v), to mimic receptive field properties, have been examined in a separate analysis.

The results of our initial modeling using this approach are shown in Figure 15, showing that including a target-target inhibitory mechanism will give a model response well matched to the experimental data. However, we hypothesize that including a stronger luminance dependent inhibition (also over a diffuse region) would also give a similar result. To determine which of these options is correct, further experiments on CSTMD will vary the size of the 2nd target distractor. If increasing the size of the distractor target decreases the strength of inhibition, then a target-target inhibitory mechanism is a more likely mechanism (accounting for temporal adaptation and receptive field integration properties). Which of these two distinct options is correct, will result in profound differences for the functional role of CSTMD.

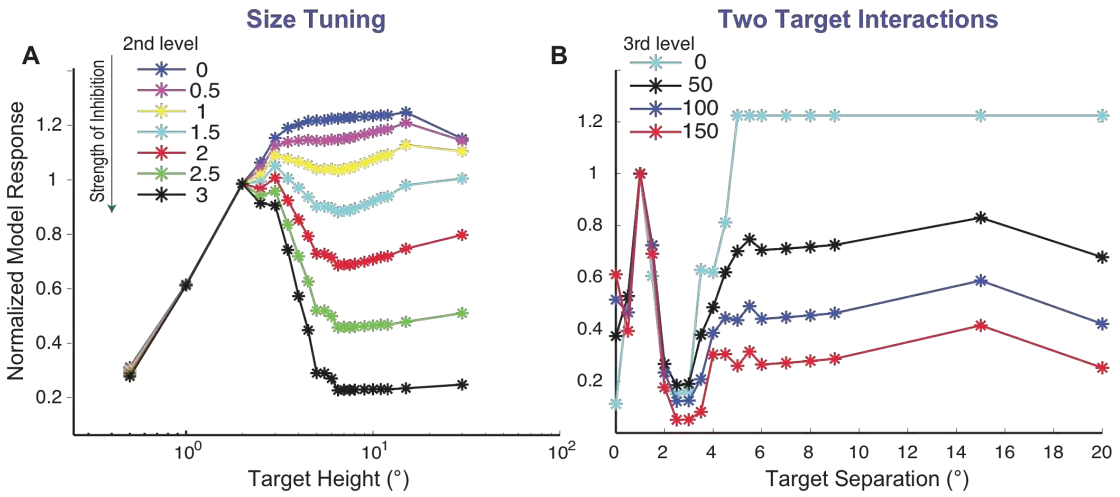

Figure 15: (A) Varying the strength of the 2nd level inhibitory surround (Fig 13-ii) produces a size tuning curve similar to the physiological observations (Fig 14A). (B) Similarly, varying the strength of 3rd level inhibition (Fig 13-iii) shows a shape well matched to the two target interactions (Fig 14 B&C).

The next challenge for this modeling effort will be to weight the local spatial summation in such a way that it reflects both the shape of the apparent receptive field of CSTMD1, and the influence of inhibition mediated beyond the classical receptive field by heterolateral interactions (i.e. the potent inhibitory input that originates in the opposite visual hemisphere). Only then will we be able to confidently explore the responses to more complex stimuli, such as the natural scenes in Figure 12. Finally, it is expected that the concepts for local facilitation described in Section 3.2.2 will be immediately applicable to the wide-field model as a part of this effort to account for spatial summation. We expect to make substantial progress with this approach in subsequent periods of the grant.

4 Personnel Supported

The personnel supported by FA9550-09-01-0116 include Dr Patrick Shoemaker, senior scientist at Tanner Research, Inc. Personnel supported by AOARD-09-4058 (FA 2386-09-1-4058) include Dr Karin Nordström (who moved to Sweden in May 2009), Dr Steven Wiederman, Mr Douglas Bolzon (PhD candidate), Mr James Dunbier (PhD candidate) & A/Prof David O'Carroll.

5 Publications

5.1 Papers Produced Under Support of this Grant:

The O'Carroll laboratory has had a very successful year in publishing data supported by this project, including a review paper published in the high impact journal Trends in Neurosciences and a full paper from the earlier work of prior Air Force funded projects looking at spatial inhibitory mechanisms completed with partial support from this present project and now published in the top ranked Journal of Neuroscience. In addition, we have one further paper on target detection in natural scenes presently in press. Several

further papers are either under review or in preparation, so we expect at least 2 further papers to be published with support from this project in the next 6 months.

Wiederman, S.D., Brinkworth, R.S.A & O'Carroll, D.C. (2010) Performance of a bio-inspired model for the robust detection of moving targets in high dynamic range natural scenes. Journal of Computational and Theoretical Nanoscience 7: 1-10 doi:10.1166/jctn.2010.1438 (in press)

*Bolzon, DM, Nordström, K & O'Carroll, DC (2009) Local and Large-Range Inhibition in Feature Detection. Journal of Neuroscience 9(45): 14143-14150; doi:10.1523/JNEUROSCI.2857-09.2009

*Nordström, K & O'Carroll, DC (2009) Feature Detection and the Hypercomplex Property in Insects. Trends in Neurosciences 32:383–391 doi:10.1016/j.tins.2009.03.004

* n.b. these papers formally acknowledge the partial support of FA 2386-09-1-4058, although the work included data from earlier work supported from other sources (also cited).

In addition, Shoemaker has continued to work on a manuscript concerning bistability and amplification mediated by NMDA receptors. It has been determined to split this work into two sequential publications; the first, detailing the results of analysis of the stationary equations, is near completion and will be submitted in the upcoming first option period of the grant.

5.2 Papers by the Principals in Related Areas:

Theobald, JC, Warrant, EJ & O'Carroll DC (2009) Wide-field motion tuning in nocturnal hawkmoths. Proceedings of the Royal Society of London B, published online before print, November 11, 2009 doi:10.1098/rspb.2009.1677

Brinkworth RSA & O'Carroll DC (2009) Robust Models for Optic Flow Coding in Natural Scenes Inspired by Insect Biology. PLoS Computational Biology 5(11):e1000555. doi:10.1371/journal.pcbi.1000555

6 Interactions / Transitions

6.1 Participation/presentation at meetings, conferences, and seminars

6.1.1 Conference Presentations / Posters Supported Directly by this Grant:

O'Carroll D.C. "Neural processing of form and motion by the insect visual system". Australia. Invited presentation, Vision 2010: From Photoreceptors to Behaviour, Friday, 29 January & Saturday, 30 January 2010, A satellite meeting to the 2010 joint meeting of the Australian Neuroscience Society and the Australian Physiological Society

Dunbier J.R., Bolzon D.M., Wiederman S.D., Shoemaker, P.A., Nordström K. & O'Carroll D.C. (2010) "Facilitation in hyperacuity of dragonfly hypercomplex neurons." Poster # POS-TUE-156, 30th Annual Meeting of the Australian Neuroscience Society, Sydney, January 2010

Barnett P.D., Nordström K. & O'Carroll D.C. (2010) Local motion detection: temporal and spatial modulation of gain and transient responses to features in natural images.

Poster # POS-MON-195, 30th Annual Meeting of the Australian Neuroscience Society, Sydney, January 2010

6.1.2 Seminars and Laboratory Meetings

O'Carroll D.C. "Frontiers of motion vision in insects: From physiology to a bionic eye" School Seminar, School of Molecular & Biomedical Sciences, University of Adelaide. 2009

O'Carroll D.C. "The insect optic lobes and insights into mechanisms underlying feature and motion vision" School of Medical Sciences seminar series, The University of Sydney, August 21, 2009

6.2 Consultative and advisory functions

None this period.

6.3 Transitions

Dr Karin Nordström obtained an early career research fellowship from the Swedish Research Council and start-up funding to establish a laboratory at Uppsala University, Sweden. She moved to take up this position in late May 2009. She has continued to contribute to experimental design and analysis of experimental data for this project and spent several weeks back in the Adelaide laboratory in January 2010 to complete some further experiments towards the project goals. We expect to maintain close collaboration with her throughout the ongoing work associated with this project, should the option periods be funded.

7 New Discoveries, Inventions, or Patent Disclosures

None this period, beyond the findings reported above.

8 Honors / Awards

None this period.

References

[1] Alaburda, A., Alaburda, M., Baginskas, A., Gutman, A., Svirskis, G. (2001) Criteria of bistability of the cylindrical dendrite with variable negative slope of N-shaped current-voltage (I-V) membrane characteristic. Biophysics-USSR 46: 337-340.

[2] Bolzon, DM, Nordström, K & O'Carroll, DC (2009) Local and Large-Range Inhibition in Feature Detection. Journal of Neuroscience 9(45): 14143-14150; doi:10.1523/JNEUROSCI.2857-09.2009.

[3] Fowler, C.E., Aryal, P., Slesinger, P.A. (2007) Evidence for association of GABA(B) receptors with Kir3 channels and regulators of G protein signaling (RGS4) proteins. Journal of Physiology 580: 51-65.

[4] Goldman, D.E. (1943) Potential, impedance, and rectification in membranes. Journal of General Physiology 27: 37-60.

[5] Geurten, BRH, Nordström, K, Sprayberry, JDH, Bolzon, DM & O'Carroll, DC (2007) Neural mechanisms underlying target detection in a dragonfly centrifugal neuron. J. Exp.Biol. 210, 3277-3284; DOI: 10.1242/jeb.008425.

[6] Gutman, A.M. (1991) Bistability of dendrites. International Journal of Neural Systems 1: 291-304.

[7] Gutman, A., Baginskas, A., Hounsgaard, J., Svirskiene, N., Svirskis, G. (2005) Semi-quantitative theory of bistable dendrites with potential-dependent facilitation. In Modeling in the Neurosciences, Reeke, Poznanski, Lindsay, Rosenberg, Sporns, eds., Taylor and Francis, Boca Raton, pp. 435-457.

[8] Jahr, C.E., Stevens, C.F. (1990) Voltage dependence of NMDA-activated macroscopic conductances predicted by single-channel kinetics. Journal of Neuroscience 10: 3178-3182.

[9] Leaney, J.L. (2003) Contribution of Kir3.1, Kir3.2A and Kir3.2C subunits to native G protein-gated inwardly rectifying potassium currents in cultured hippocampal neurons. European Journal of Neuroscience 18: 2110-8.

[10] Mah, EL, Brinkworth, RSA & O'Carroll DC (2008) Implementation of an Elaborated Neuromorphic Model of a Biological Photoreceptor. Biol. Cybern. 98: 357-369.

[11] Mel, B.W. (1992) NMDA-Based pattern discrimination in a modeled cortical neuron. Neural Computation 4: 502-516.

[12] Mel, B.W. (1993) Synaptic integration in an excitable dendritic tree. Journal of Neurophysiology 70: 1086-1101.

[13] Nordström, K & O'Carroll, DC (2009) Feature Detection and the Hypercomplex Property in Insects. Trends in Neurosciences 32:383–391; doi:10.1016/j.tins.2009.03.004.

[14] Polsky, A., Mel, B.W., Schiller, J. (2004) Computational subunits in thin dendrites of pyramidal cells. Nature Neuroscience 7: 621-627.

[15] Sodickson, D.L., Bean, B.P. (1996) Neurotransmitter activation of inwardly rectifying potassium currents in dissociated hippocampal CA3 neurons: interactions among multiple receptors. Journal of Neuroscience 16: 6374-6385.

[16] Wiederman, S.D., Brinkworth, R.S.A & O'Carroll, D.C. (2010) Performance of a bio-inspired model for the robust detection of moving targets in high dynamic range natural scenes. Journal of Computational and Theoretical Nanoscience 7: 1-10; doi:10.1166/jctn.2010.1438 (in press).

[17] Wiederman, S.D., Shoemaker, P.A., and O'Carroll, D.C. (2008) A model for the detection of moving targets in clutter inspired by insect physiology. *PLoS ONE*, Vol. 3(7): e2784. doi:10.1371/journal.pone.0002784.